1-4-2017

Effect of trehalose as an additive to dimethyl sulfoxide solutions on ice formation, cellular viability, and metabolism.

Jason Solocinski
University of Michigan - Dearborn

Quinn Osgood
University of Michigan - Dearborn

Mian Wang
University of Michigan - Dearborn

Aaron Connolly
University of Michigan - Dearborn

Michael A. Menze
University of Louisville

See next page for additional authors

Original Publication Information

Solocinski, Jason, et al. "Effect of Trehalose as an Additive to Dimethyl Sulfoxide Solutions on Ice Formation, Cellular Viability, and Metabolism." 2017. *Cryobiology* https://doi.org/10.1016/j.cryobiol.2017.01.001

Effect of Trehalose as an Additive to Dimethyl Sulfoxide Solutions on Ice Formation, Cellular Viability, and Metabolism

Jason Solocinski[1], Quinn Osgood[1], Mian Wang[1,3], Aaron Connolly[1], Michael A. Menze[2], Nilay Chakraborty[1]

[1]Department of Mechanical Engineering, University of Michigan-Dearborn
4901 Evergreen Road, Dearborn MI 48128, Unites States
[2]Department of Biology, University of Louisville, Louisville, KY 40292, Unites States
[3]Current Address: Department of Mechanical Engineering, University of Minnesota, Minneapolis, MN 55455, Unites States
Address for reprint requests and other correspondence: Nilay Chakraborty and Michael A. Menze Tel.: 313-583-6788, Fax: 313-593-3851, Email: nilay@umich.edu; Tel.: (502) 852-8962, Fax: 502- 852-0725, Email: michael.menze@louisville.edu

Keywords: Hepatocellular Carcinoma Cells, Cryopreservation, Raman Microspectroscopy, Respiration, Osmotic Stress, Mitochondria

Abstract

Cryopreservation is the only established method for long-term preservation of cells and cellular material. This technique involves preservation of cells and cellular components in the presence of cryoprotective agents (CPAs) at liquid nitrogen temperatures (-196°C). The organic solvent dimethyl sulfoxide (Me_2SO) is one of the most commonly utilized CPAs and has been used with various levels of success depending on the type of cells. In recent years, to improve cryogenic outcomes, the non-reducing disaccharide trehalose has been used as an additive to Me_2SO-based freezing solutions. Trehalose is a naturally occurring non-toxic compound found in bacteria, fungi, plants, and invertebrates which has been shown to provide cellular protection during water-limited states. The mechanism by which trehalose improves cryopreservation outcomes remains not fully understood. Raman microspectroscopy is a powerful tool to provide valuable insight into the nature of interactions among water, trehalose, and Me_2SO during cryopreservation. We found that the addition of trehalose to Me_2SO based CPA solutions dramatically reduces the area per ice crystals while increasing the number of ice crystals formed when cooled to -40 or -80 °C. Differences in ice-formation patterns were found to have a direct impact on cellular viability. Despite the osmotic stress caused by addition of 100mM trehalose, improvement in cellular viability was observed. However, the substantial increase in osmotic pressure caused by trehalose concentrations above 100mM may offset the beneficial effects of changing the morphology of the ice crystals achieved by addition of this sugar.

1. Introduction

Cryoprotective agents (CPAs), are traditionally used to ensure survival of cellular samples at cryogenic temperatures. Due to toxicity concerns of penetrating CPAs such as dimethyl sulfoxide (Me_2SO), several additives such as glycerol [1], disaccharides (e.g. trehalose, sucrose [1; 2; 3]), amino acids (e.g. proline [2; 4; 5]), and proteins (e.g. sericin [6]) have been used in recent years. Several organisms in nature are frequently exposed to subzero temperatures and a common strategy in these organisms is to accumulate biocompatible osmolytes such as trehalose before the onset of water loss due to freezing, drying, or both [7; 8; 9]. Trehalose has been found to improve the cryogenic outcome in a variety of biological materials including mammalian cells and cellular monolayers [4; 5; 10; 11; 12]. However, the actual mechanism for improvement of cellular viability in presence of trehalose following cryopreservation remains poorly understood [13; 14]. Here, we present an in-depth analysis of the effect of trehalose addition to a Me_2SO-based freezing solution on ice-formation, cumulative osmotic stress, viability, and post-thaw metabolic activity of human hepatocellular carcinoma (HepG2) cells.

At low cooling rates (~1°C /min) ‘solution effects’ injury stemming from exposure of cells to a hypertonic extracellular environment for extended period of time is the primary cause of cellular damage [15; 16; 17; 18]. During freezing, water crystalizes in the extracellular environment – a process that increases the solute concentration in the non-frozen water fraction surrounding the cells. In addition to osmotic stress, extracellular ice morphology can have a strong bearing on cellular viability [19]. However, most experimental techniques do not allow characterizing spatial differences in ice morphology and solute distribution in frozen systems. Spatially correlated Raman microspectroscopy

techniques were used at -40 and -80 °C to characterize changes in the ice formation and solute distribution after addition of trehalose to Me_2SO based freezing solutions.

Vibrational Raman microspectroscopy is a highly sensitive technique that relies on detection of vibration in molecular moieties when excited with laser irradiation [20; 21]. Since the vibrational information is specific to the chemical bonds and symmetry of molecules, Raman microspectroscopy provides a fingerprint by which a molecule can be identified [21; 22]. This extends to different physical states in the same molecule such as the transition from water to ice [23; 24]. Therefore, it is feasible to use Raman microspectroscopy to study cryoprotective formulations and investigate the distribution, state, and concentration of compounds at different sub-zero temperatures. While Me_2SO has been widely used as a penetrating cryoprotectants and is known to depress the freezing point of aqueous solutions [25; 26], at relatively low concentration (<1M) Me_2SO has little influence on the average water-water hydrogen bonding strength [27]. In contrast to Me_2SO, Raman microspectroscopic observations [28] and molecular dynamic simulations [29; 30] have revealed that trehalose promotes a destructive effect on the tetrahedral hydrogen-bond network of pure water [30]. These studies suggest that in presence of trehalose, water binds stronger to the sugar than to other water molecules. Trehalose obstructs the water-crystallization process, thereby destroying the water network and forming a sugar-water network [31]. At low temperatures formation of ice creates a partially dehydrated environment and while the additive trehalose may be excluded from the immediate vicinity of the biomolecules of interest [32] in presence of the sugar, ice formation occurs at lower temperatures but at more independent nucleation sites [33].

We hypothesized that the destructuring effect of trehalose on water-water hydrogen bonding will be maintained in presence of Me_2SO. Therefore, by reducing the availability of water molecules to join a tetrahedral hydrogen network that plays a formative role in creating ice crystals during freezing, an overall smaller ice crystal size may be observed in presence of water, trehalose, and M_2SO compared to the binary water Me_2SO system. In this study a highly sensitive confocal Raman microspectroscopic (CRM) system was used to generate spatially correlated chemical maps of the distribution of ice, Me_2SO, and trehalose in the frozen systems. Special attention was paid to the effect of trehalose concentration on the formation and distribution of ice crystals and the recovery of metabolic functions after cryopreservation of HepG2 cells.

2. Materials and Methods

2.1 Sample preparation

Low endotoxin α, α-trehalose dihydrate was obtained from Pfanstiehl Inc. (Waukegan, IL) and dimethyl sulfoxide (Me_2SO) was procured from Sigma Aldrich (St. Louis, MO). Solutions of 10% (v/v) Me_2SO were made by mixing 10% pure Me_2SO with 90% phosphate buffered saline (PBS) solution from Sigma Aldrich (St. Louis, MO) volume by volume and then dissolving trehalose to reach final concentrations of 0mM, 100mM, and 300mM trehalose. These solutions were used in the confocal Raman microspectroscopy studies and in the cell freezing studies.

2.2 Low temperature confocal Raman microspectroscopy

Low temperature Raman measurements were conducted using a customized confocal microscope and Raman spectrometer combination (UHTS 300, WITec Instruments Crop, Germany). Raman spectra were collected using a highly sensitive EMCCD camera (Andor Technology, UK). A 532nm solid-state laser was used for excitation and images were captured using a 10X objective (Carl Zeiss, Germany). A liquid nitrogen cooled freezing stage (FDCS 196, Linkam Scientific Instrument, UK) was integrated with the microscopy setup and was used to cool the samples at a predetermined rate. For each experiment, the freezing stage with 20µl solution of sample was mounted on the Raman microscope stage with a custom-made stage adaptor. Samples were cooled to -40 and -80 °C at a rate of 1°C/min, and then held for approximately 10 minutes at each temperature before the spectral information was collected. Spatially correlated hyperspectral Raman images were created using the

Raman signals collected from a window of 50×50μm. Each array of Raman scans was collected using a low integration time (0.3s) to minimize impact of laser irradiation on the ice crystals formed. Each experiment was repeated 3 times and the confocal Raman images presented here are representative for all 3 repetitions.

2.3 Image Processing

Images were processed using the open source software Image J [34]. All images were processed for identification and quantification of ice crystals using a standard bandpass filter for particle analysis. A threshold was applied to convert raw hyperspectral images to a binary image. The Watershed segmentation algorithm [35] in Image J was used to prevent the individual ice crystals from merging to one another and the Particle Analysis tool was used to quantify both the number and area of the ice crystals.

2.4 Cell culture and cryopreservation

Human hepatocellular carcinoma (HepG2) cells were obtained from the American Type Culture Collection (Manassas, VA), and grown in 75 cm^2 cell culture flasks (Corning Incorporated, Corning, NY). Standard culture medium for HepG2 cells was composed of Opti-MEM I (Gibco, Carlsbad, CA) supplemented with 10% fetal bovine serum (FBS) (Gibco) and penicillin-streptomycin solution to yield final concentrations of 100 units/mL penicillin G and 100 μg/mL streptomycin sulfate (HyClone-Thermo Scientific, Logan, UT). Cells were cultured at 37°C in a humidified atmosphere of 5% CO_2 and 95% air. Upon reaching 80-90% confluency, cells were dissociated using 0.25% trypsin plus 1mM EDTA in a balanced salt solution for 10 min, and trypsin activity was stopped by adding fully supplemented medium to the flask followed by centrifugation for 5 min at 200 x g. The

cells were washed once with fully supplemented medium and the final cell pellet was resuspended in one of the three different solutions containing CPAs previously mentioned. Cell samples were diluted in the CPA solutions to a concentration of 1 x 10^6 cells/mL. A volume of 1mL of the samples was transferred into type D micro tubes (Sarstedt, Radnor, PA), and placed into a passive freezing device (Cool Cell LX, Biocision, Menlo Park, CA), which provides a cooling rate of 1°C/min. After loading with samples, the freezing device was quickly transferred to a -80°C commercial freezer for 24h. The following day, the tubes were quickly collected and transferred to a LN2 storage container.

2.5 Mathematical modeling of cumulative osmotic stress

The progressive loss of osmotically active intracellular water with the increase of extracellular osmolality during freezing at 1°C/min was modeled based on the formulation as discussed by Fahy, 1981. The cumulative osmotic stress experienced by the cell was defined as loss of osmotically active water volume over time. The differential decrease in osmotically active volume of intracellular water with change of temperature was indicated by following equation (Fahy, 1981):

$$\frac{dV}{dT} = \frac{-L_p A R T_k^2 (T - T_b)}{B V \bar{V}_w} \times \ln\left[\frac{1 - \left(\frac{V}{(V_b/\bar{V}_w + 1)}\right) - \left(\frac{V}{(V_b/\bar{V}_w + 1)^2}\right)}{1 + 0.00966T + 4.1025 \times 10^{-5} T^2}\right]$$

Here A is the total surface area of the cell, L_p is the hydraulic conductivity of the cell membrane at a given temperature T_k, R is the universal gas constant, B is the cooling rate, b is the temperature coefficient of the hydraulic conductivity, $\bar{V}_w$ is the partial molar volume of the water, V is the volume of intracellular water, and V_b is the number of moles

of solute in the cells. Relevant parametric values for HepG2 cells are listed in Table 1. S and I are parameters that are dependent on the non-aqueous mole fraction of the constituents of the freezing medium. The following parametric relationships were used for calculating S and I for each of the CPA formulations with trehalose.

$$\square = 3.55\,\square_{\square} + 1.8 \text{ and } \square = 0.076\square_{\square} + 0.86 \text{ where } \square_{\square} = \square_{\square}/(\square_{\square} + 2\square_{\square} + \square_{\square})$$

Here, $\square_{\square}$ is the number of moles of Me_2SO, $\square_{\square}$ is the number of moles of salts in the freezing solution and finally, $\square_{\square}$ is the number of moles of trehalose in the freezing solution. The calculated values for the parameters S and I are presented in Table 2 for each of the CPA formulations. A computer code written in Mathematica 8 (Wolfram Research, Champaign, IL) was used to solve the set of equations described above.

2.6 Post-thaw viability and metabolic profile analysis

Following storage over LN2 for a day, individual microtubes were collected and quickly warmed to physiological temperature using a water bath maintained at 37°C. In order to remove the CPAs in the solution, cells were collected using centrifugation followed by resuspension in standard culture medium. Cells were enumerated with a Bright Line™ hemocytometer (Hausser Scientific, Horsham, PA) and membrane integrity was assessed using trypan blue exclusion assay. The oxygen consumption rates (OCRs) of HepG2 cells cryopreserved under different CPA conditions were measured using the XFp Extracellular Flux Analyzer (Seahorse Biosciences, North Billerica, MA) on days 1 and 3 post thawing. The Seahorse XFp analyzer operates by creating a transient chamber so that cellular oxygen consumption rates can be monitored. Post thaw cell samples were plated on XFp plates at $4x10^4$ cells per well and incubated for 24h before respiration rates

were measured. Preceding experimentation, the XFp cartridges (Seahorse Bioscience, North Billerica, MA) were hydrated with XFp calibrant (Seahorse Bioscience) and stored at 37°C for 24h. One-hour prior measuring cellular respiration, the cell culture media was aspirated from the individual culture wells and a medium containing DMEM (Dulbecco's Modified Eagle's medium, Seahorse Bioscience) plus 2mM L-Glutamine and 20mM glucose (Sigma Aldrich, St. Louis, MO) was added. The plate was maintained for 1h at 37°C and ambient atmosphere. The XFp cartridge was loaded with a suite of reagents yielding the following final concentrations in the cell sample: oligomycin (1µM), carbonyl-cyanide-4-(trifluoromethoxy) phenylhydrazone (FCCP, 0.5µM), and rotenone/antimycin A (0.5µM). Oligomycin acts as F_0F_1-ATPase inhibitor and oxygen consumption rates measured in presence of this inhibitor indicate mitochondrial leak respiration, while FCCP acts as an uncoupling agent which collapses the mitochondrial proton gradient and thereby uncouples the oxidation system from the phosphorylation system, maximizing oxygen consumption rates. To estimate the contribution of non-mitochondrial processes to overall oxygen flux, rotenone and antimycin A were added to inhibit complex I and III of the respiratory system.

2.7 Statistical analysis

Data were analyzed with a student t-test. Excel 2013 (Microsoft, Redmond, WA) and Origin Pro (Northampton, MA) were used for the analyses. Data sets are presented as mean ± (SEM).

3. Results

3.1 Confocal Raman microscopy (CRM)

Spatially correlated CRM can be used for simultaneous identification and localization of multiple molecular moieties by analyzing individual chemical signatures. In Fig. 1, a typical Raman spectrum of our tertiary ice, trehalose, and Me_2SO system is used to spatially correlate the distribution of compounds in a 50x50 μm^2 sample window at -40°C. The hyperspectral images were extracted using the appropriate characteristic wavelengths for each of the compounds and brightness correlates with increased compound concentration. It is interesting to note that channels of high Me_2SO concentrations were found to be embedded between ice crystals while trehalose seems to be more ubiquitously distributed throughout both the ice and Me_2SO rich regions of the sample.

In this study, primary emphasis was laid on investigating the ice-formation characteristics at different trehalose concentrations with decreasing temperature. As shown in Fig. 2, ice crystals (bright area) were surrounded by narrow channels (dark area), which are rich in Me_2SO due to the presence of the solutes rejected by the nucleating and growing ice phase. Average ice crystal area was determined and a clear trend in formation of ice crystals having smaller surface areas with increase in trehalose concentration and decrease in temperature was observed. At -40°C in samples containing 10% Me_2SO alone relatively large ice crystals (A_{avg}= 138.2 μm^2) with sharp and angular boundaries developed. Upon addition of 100mM trehalose to 10% Me_2SO, ice crystals were smaller (A_{ave}= 114.9 μm^2) than in presence of 10% Me_2SO alone. Furthermore, the ice crystals displayed more rounded and smoother boundaries. Further increases in

229 trehalose concentration to 300mM, caused additional decreases in ice crystal area (A_{ave}=
230 54.3 μm^2) and boundaries appear to be more rounded than under the two other conditions
231 investigated. Upon cooling to -80°C, all the samples exhibit additional decreases in
232 average ice crystal size compared to -40°C. At -80°C the ice crystals had a relatively
233 uniform distribution, and the same decreasing trend of ice crystal area with increasing
234 trehalose concentrations found for samples at -40°C, was observed. It is noteworthy that
235 for 10% Me_2SO plus 300mM trehalose at -80°C, the structure of ice crystals is very
236 different compared to all other conditions and the ice crystals were extremely small (A_{ave}=
237 19.8μm^2) forming a more network-like structure.

238 Based on the morphology and number of ice crystals in the hyperspectral images
239 the average size distribution and frequency of crystals per unit of viewing area was
240 calculated. As shown in Fig. 3A, ice crystal area decreases while the number of ice
241 crystals per unit viewing area increases with increasing trehalose concentration. This
242 effect was observed at both temperatures, but the increase in number of ice crystals with
243 increase in trehalose concentration was most pronounced at -80°C (Fig. 3B). While a
244 similar trend in crystal formation was observed in absence of Me_2SO and in presence of
245 only trehalose the crystal sizes are significantly bigger (Supplementary Figures I and II),
246 indicating that addition of Me_2SO does in fact play an important role in determining and
247 reducing the size of the ice crystals formed.

248 Ice formation in the extracellular environment increases the solute concentration
249 in the unfrozen section around the cells. While Me_2SO is a penetrating cryoprotectant,
250 trehalose remains predominantly outside the cell contributing to the increasing
251 extracellular solute concentration [26; 36]. These freezing events outside the cellular

environment have a direct impact on the osmotically active cell volume as cells maintain an osmotic equilibrium with the extracellular environment [37]. Guided by the hydraulic conductivity of the cell membrane and the rate of decrease in temperature, cells become partially dehydrated due to osmotically active water leaving the cytoplasm and organelles [38]. At low cooling rates, such dehydration can lead to osmotic stress mediated injury in cells commonly known as 'solution effects' injury [16; 39], and can be considered as the predominant injury mechanism at low cooling rates [40]. Such injury can be mathematically modeled as the cumulative effect of volumetric reduction of cells owing to the loss of water [40]. Fig. 4 describes the relationship between temperature and osmotically active cell volume. As expected, at a freezing rate of 1°C/min, we see that cumulative osmotic stress increases substantially starting at -15°C when frozen in a 10% Me_2SO solution. Addition of trehalose to 10% Me_2SO solution increases the cumulative osmotic stress experienced by cells (Fig. 5). As expected, we see that upon addition of 300 mM trehalose cells experience increased reduction of osmotically active water volume leading to higher cumulative osmotic stresses (Fig. 5). According to the model developed here, most of the injuries occur in -5 to -20°C range where there is a substantial difference in percent increase of cumulative osmotic stress when 300 mM trehalose is added to Me_2SO.

3.2 Cell growth and metabolic profile analysis

Membrane integrity after freeze thawing and growth of HepG2 cells was measured in order to assess the physiological consequences of trehalose addition to the CPA solution. Despite the increase in cumulative osmotic stress in presence of 100mM trehalose compared to Me_2SO alone, membrane integrity was significantly higher for cells

frozen in presence of 100mM trehalose compared to 0mM trehalose (Fig. 6A). Furthermore, no significant differences in growth behavior were found between cells frozen without trehalose or in presence of 100mM of the sugar (Fig. 6B). After an initial lagging phase of about 3 days, cell numbers increased rapidly over the next 2-3 days, followed by reduced proliferation rates due to contact inhibition. However, due to the substantial higher cumulative osmotic stress experienced at 300mM trehalose, cells frozen in this CPA showed both lower membrane integrity and longer delayed growth performance compared to the 100mM trehalose samples (Fig. 6A, B). Oxygen consumption rates (OCR) provided an additional appraisal of cellular functions of cells after cryopreservation. In agreement with growth performance, analysis of the basal OCR data for each CPA condition on days 1 and 3 post-thawing showed increases in cellular respiration over time for each CPA employed (Fig. 7A). Increases in OCR were followed by increases in oligomycin inhibited and FCCP uncoupled respiration rates (Fig. 7B, C). Furthermore, a slight increase in the background oxygen flux after addition of rotenone and antimycin-a was also observed (Fig. 7D). In summary, no substantial differences in bioenergetic parameters were observed for cells frozen in the three different CPAs after 3 days of cell recovery.

4. Discussion

The rate of freezing is a critical factor that determines the nature and extent of cellular injury during cryoprocessing. At slow freezing rates (1 - 10 °C/min) physical damage by advancing ice crystals and prolonged exposure to hyperosmotic conditions are the dominant injury mechanisms. On the other hand, at fast freezing rates (>10 °C/min) intracellular water fails to equilibrate with the rapidly increasing extracellular osmolality due to physical limits associated with the hydraulic conductivity of the cell membrane and the chances of formation of highly lethal intracellular ice increases [41; 42].

Irrespective of the specific freezing rates, CPAs offer protective mechanisms to prevent cellular injury during freezing. CPAs capable of permeating the cell membrane (i.e. Me_2SO) play a role in preventing intracellular ice formation and are thought to contribute to a vitrified environment in the intracellular space, whereas non-penetrating cryoprotectants (i.e. polyethelene glycol) modulate the extracellular ice formation characteristics [43] and are known to have osmolytic properties preventing membrane damage caused by hyperosmotic conditions in the extracellular environment during freezing [16]. One of the most significant drawbacks associated with use the of CPAs is the fact that many CPAs, including the widely used compound Me_2SO, are known to have significant cytotoxic effects both in short term and long term. Me_2SO has been reported to cause translocation of apoptosis-inducing factors from mitochondria to nucleus and poly-(ADP-ribose)-polymerase (PARP) activation [44]. Additionally, Me_2SO is reported to induce pore formation in plasma membrane [45]. The toxicity associated with CPAs has been a limiting step for the use of high CPA concentrations, and poses a significant problem for application of cryopreservation protocols to a wide variety of cells including

316 stem cells. At higher concentrations of Me_2SO, Molecular Dynamics (MD) simulations
317 predict cell membrane loosening, pore formation, and eventual bilayer collapse [46].

318 One strategy to mitigate the risk of using toxic CPAs is to add cosolutes with
319 cytoprotective properties as additives to the CPA formulation. While many additives have
320 been used as cryoprotectants, it has been demonstrated that a majority of them fail to
321 protect proteins and phospholipid bilayers from denaturation during dehydration stress
322 experienced by cells during cryoprocessing [47]. It is interesting to note that disaccharides
323 such as sucrose and trehalose are an exception and possess the ability to prevent protein
324 denaturation and membrane fusion during cryoprocessing [1; 48]. Trehalose have been
325 widely used as additives to cryoprotectants formulations in recent years [2; 3; 49; 50].
326 Trehalose is a non-reducing disaccharide and it has been linked to extreme dehydration
327 and low temperature tolerance in several cryptobiotic organisms [51]. Addition of 0.2-
328 0.6M trehalose to a CPA containing 10% Me_2SO has been demonstrated to increase both
329 post-thaw cell viability and plating efficiency in several mammalian cell types including
330 primary human hepatocytes [52], human embryonic cells [10], and pancreatic islets [53].
331 However, the exact mechanism(s) by which trehalose protects cellular structures during
332 cryopreservation remains unclear.

333 Due to the lack of dedicated trehalose transporter in mammalian cells, addition of
334 trehalose to CPA formulations results in presence of trehalose predominantly in the
335 extracellular space. The water replacement hypothesis [54] suggests that the hydroxyl
336 groups of trehalose can substitute for the hydrogen bonding of water [5]. During
337 cryopreservation as water molecules are being progressively removed from extracellular
338 environment due to ice formation, trehalose may play a critical role in maintaining the

integrity of the phospholipid structure of the cell membrane. In a comparable system involving water loss, such as drying, it has been demonstrated that the loss of the hydration effect of water is compensated by the presence of trehalose, thus preserving the phospholipid bilayer. However, without trehalose, it has been found that desiccation leads to heterogeneities in phospholipid packing and reduced acyl chain density, thereby destabilizing the membrane and resulting in damage upon the influx of water [55]. As an additive to CPA formulations, trehalose may play a similar role in minimizing cellular injury during the partial dehydration created during cryoprocessing owing to the progressive ice formation in extracellular space [56]. However, it needs to be noted that to offer maximal protection during desiccation, trehalose has to be present on both sides of the plasma membrane [14], which is not the case without a sugar loading strategy.

By employing Raman microspectroscopy we found that in absence of sugar loading trehalose may exert a protective effect by modulating the nature of the extracellular ice crystal formed (Fig. 1). Trehalose has been known to inhibit ice crystal growth [33], and recent studies underscore a strong correlation between the ice-crystal size and cell lethality [57]. Rapid growth of large ice crystals in extracellular medium increases the possibility of damage to the cell membrane from advancing ice crystals. In this study we demonstrate that presence of trehalose as an additive to the CPA formulation can significantly influence the morphology, shape, and size of ice crystal formation (Fig. 2) – which can in turn have a significant role to mitigate physical damage due to advancing ice crystals during freezing. While similar studies have been reported using optical microscopy [58], field emission electron microscopy systems including cryoscanning electron microscopy (SEM), or transmission electron microscopy (TEM)

[33], only the hyperspectral imaging technique using spatially correlated Raman microspectroscopy system combines digital imaging and molecular/elemental spectroscopy for material analysis. This technique provides the significant advantage of spectroscopically identifying the true nature of ice formation pattern. The ice crystal formation is indicated by appearance of a distinct peak in the symmetric spectral region of the OH stretching peak ~ 3130 cm^{-1} wavenumbers [5; 59].

At low temperatures both the reduction in the free water, indicated by decreasing intensity of the asymmetric portion of the OH stretching spectra (centered ~3435 cm^{-1}), and enhancement of nucleation sites for ice crystals have been theorized to limit the number of ice crystals in presence of trehalose. Hyperspectral images of the ice crystals formed at both -40°C and -80°C both support this theory. The number of nucleation sites indicated by the number of ice crystals increase significantly when 300mM trehalose in added to the CPA solution. As temperature of the system is lowered at 1°C/min to -80°C, this effect is significantly enhanced in comparison to the number of ice crystals formed at -40^{o}C. Systematic quantification of the ice crystal number and area as seen on the hyperspectral images indicates that the number of ice crystals increases rapidly, and the area per ice crystal decreases in turn (Figs. 3A, B). Surprisingly, while cumulative osmotic stress increases with increasing trehalose concentrations (Figs. 4,5) membrane integrity and metabolic activity is not negatively impacted (Figs. 6,7). These findings reinforce the notion that ice crystal structure has direct impacts on cryopreservation outcomes and can be modulated by the addition of sugar additives to the CPA solution. Experiments with mesenchymal stem cell cells that are more sensitive to osmotic stress than HepG2 cells are currently underway and should provide additional insights into the complex

385 relationship between osmotic stress, ice-crystal morphology, and viability post thawing in
386 cryopreservation.

Conflict of interest

The authors certify that they have no affiliations with or involvement in any organization or entity with any financial interest (such as honoraria; educational grants; participation in speakers' bureaus; membership, employment, consultancies, stock ownership, or other equity interest; and expert testimony or patent-licensing arrangements), or non-financial interest (such as personal or professional relationships) in the subject matter or materials discussed in this manuscript.

Statement of funding

This research was funded by NSF grant numbers SusChEM 1510072 and CHE 1609440 to N.C. and IOS-1659970 to M.A.M. UM Research grant having project numbers U038727, U051381, and U046888 are also acknowledged.

Acknowledgments

The authors would also like to acknowledge Tavis Ezell's help in procuring the Raman instrumentation from WITec Instruments, GmbH.

Figure legends

Fig. 1. A solution of 10% Me_2SO and 100mM trehalose was frozen to -40°C at 1°C/min. Upon reaching stable crystal morphologies, individual hyperspectral images indicating spatial concentrations of ice, Me_2SO, and trehalose were extracted by integrating representative characteristic Raman peaks. The characteristic Raman peaks for each of the components are labeled in the average spectrum of the scanned area. (Ice: 3130 cm^{-1}, Me_2SO: 1426 cm^{-1}, trehalose: 855 cm^{-1}). Maximum intensities for each integrated peak relative to zero were 685.3, 108.2, and 22.9 CCD cts for ice, Me_2SO, and trehalose, respectively.

Fig. 2. Confocal Raman hyperspectral images of 10% Me_2SO solution in presence of 0mM, 100mM and 300mM trehalose at -40°C and -80°C. All the images are generated by integrating the ice peak (3130 cm^{-1}) from the corresponding Raman spectra.

Fig. 3. Numerical representation of crystal morphological properties extracted from Raman hyperspectral images**.** Images were taken at -40°C and -80°C for each of the three CPA solutions containing 10% Me_2SO solution with trehalose additives (0mM, 100mM, and 300mM). Hyperspectral images were analyzed with ImageJ to extract average number of ice crystals (A) and average area per ice crystals (B) were found via ImageJ per sample window (n = 3).

Fig. 4. Normalized cell volume and cumulative osmotic stress at a cooling rate of 1°C/min. Mathematica modeled parametric curves showing interaction of osmotically active cell volume and cumulative osmotic stress from 0°C to -80°C. The osmotically active volume of the cell is approximately 30% of the total cell volume.

Fig. 5. Percent increase in cumulative osmotic stress with decreasing temperature. Percent increase in cumulative osmotic stress for the 100mM trehalose and 300mM trehalose curves relative to 0mM added trehalose. A magnified inset is provided to show the largest difference occurs at the onset of freezing ranging from approximately -3°C to -20°C.

Fig. 6. Membrane integrity and growth pattern of cells after cryopreservation**.** A) Membrane integrity measured immediately after thawing (*, $p<0.01$) and B) cell grow-out after the LN2 storage for each CPA with sigmoidal fits to highlight growth patterns (n= 4, ±SEM).

Fig.7. Recovery of cellular respiration over 3 days after cryopreservation. A) basal respiration rate of cells, B) proton leak related respiration rates, C) FCCP uncoupled maximum respiration, and D) non-mitochondrial oxygen consumption (n = 3-6, ±SEM).

Supplementary Figure I: Confocal Raman hyperspectral images of ice formation in presence of 100mM and 300mM trehalose at -40°C and -80°C. The images are generated by integrating the ice peak (~3130cm^{-1}) from the corresponding Raman spectra.

Supplementary Figure II: Numerical representation of crystal morphological properties extracted from Raman hyperspectral images**.** Images were taken at -40°C and -80°C for each of the two CPA solutions containing only trehalose (100mM, and 300mM). Hyperspectral images were analyzed with ImageJ to extract average number of ice crystals (A) and average area per ice crystals (B) were found via ImageJ per sample window (n = 3).

References:

[1] T.J. Anchordoguy, A.S. Rudolph, J.F. Carpenter, and J.H. Crowe, Modes of interaction of cryoprotectants with membrane phospholipids during freezing. Cryobiology 24 (1987) 324-331.

[2] A.S. Rudolph, and J.H. Crowe, Membrane stabilization during freezing: The role of two natural cryoprotectants, trehalose and proline. Cryobiology 22 (1985) 367-377.

[3] J.P. Rodrigues, F.H. Paraguassú-Braga, L. Carvalho, E. Abdelhay, L.F. Bouzas, and L.C. Porto, Evaluation of trehalose and sucrose as cryoprotectants for hematopoietic stem cells of umbilical cord blood. Cryobiology 56 (2008) 144-151.

[4] B. Stokich, Q. Osgood, D. Grimm, S. Moorthy, N. Chakraborty, and M.A. Menze, Cryopreservation of hepatocyte (HepG2) cell monolayers: Impact of trehalose. Cryobiology 69 (2014) 281-290.

[5] T.L. Bailey, M. Wang, J. Solocinski, B.P. Nathan, N. Chakraborty, and M.A. Menze, Protective effects of osmolytes in cryopreserving adherent neuroblastoma (Neuro-2a) cells. Cryobiology 71 (2015) 472-480.

[6] T. Isobe, Y. Ikebata, T. Onitsuka, L.T.K. Do, Y. Sato, M. Taniguchi, and T. Otoi, Cryopreservation for bovine embryos in serum-free freezing medium containing silk protein sericin. Cryobiology 67 (2013) 184-187.

[7] J.D. Gantz, and R.E. Lee Jr, The limits of drought-induced rapid cold-hardening: Extremely brief, mild desiccation triggers enhanced freeze-tolerance in Eurosta solidaginis larvae. Journal of Insect Physiology 73 (2015) 30-36.

[8] J.H. Crowe, L.M. Crowe, W.F. Wolkers, A.E. Oliver, X. Ma, J.-H. Auh, M. Tang, S. Zhu, J. Norris, and F. Tablin, Stabilization of Dry Mammalian Cells: Lessons from Nature. Integrative and Comparative Biology 45 (2005) 810-820.

[9] P. Alpert, The Limits and Frontiers of Desiccation-Tolerant Life. Integrative and Comparative Biology 45 (2005) 685-695.

[10] S.S. Buchanan, S.A. Gross, J.P. Acker, M. Toner, J.F. Carpenter, and D.W. Pyatt, Cryopreservation of stem cells using trehalose: evaluation of the method using a human hematopoietic cell line. Stem Cells Dev 13 (2004) 295-305.

[11] Y.-A. Lee, Y.-H. Kim, B.-J. Kim, B.-G. Kim, K.-J. Kim, J.-H. Auh, J.A. Schmidt, and B.-Y. Ryu, Cryopreservation in Trehalose Preserves Functional Capacity of Murine Spermatogonial Stem Cells. PLoS ONE 8 (2013) e54889.

[12] A. Eroglu, M.J. Russo, R. Bieganski, A. Fowler, S. Cheley, H. Bayley, and M. Toner, Intracellular trehalose improves the survival of cryopreserved mammalian cells. Nature biotechnology 18 (2000) 163-167.

[13] J.H. Crowe, Trehalose as a "chemical chaperone": fact and fantasy. Adv Exp Med Biol 594 (2007) 143-58.

[14] J.H. Crowe, L.M. Crowe, A.E. Oliver, N. Tsvetkova, W. Wolkers, and F. Tablin, The trehalose myth revisited: introduction to a symposium on stabilization of cells in the dry state. Cryobiology 43 (2001) 89-105.

[15] J.G. Baust, D. Gao, and J.M. Baust, Cryopreservation: An emerging paradigm change. Organogenesis 5 (2009) 90-96.

[16] H.T. Meryman, R.J. Williams, and M.S. Douglas, Freezing injury from "solution effects" and its prevention by natural or artificial cryoprotection. Cryobiology 14 (1977) 287-302.

[17] G. Rapatz, and B. Luyet, Combined effects of freezing rates and of various protective agents on the preservation of human erythrocytes. Cryobiology 4 (1968) 215-22.

[18] P. Mazur, Life in the frozen state. Principles of Cryobiology. CRC Press, Boca Raton, FL, USA. Academic Press. Boca Raton (2004) 3-65.

[19] H. Takamatsu, and S. Zawlodzka, Contribution of extracellular ice formation and the solution effects to the freezing injury of PC-3 cells suspended in NaCl solutions. Cryobiology 53 (2006) 1-11.

[20] G.J. Puppels, F.F.M. de Mul, C. Otto, J. Greve, M. Robert-Nicoud, D.J. Arndt-Jovin, and T.M. Jovin, Studying single living cells and chromosomes by confocal Raman microspectroscopy. Nature 347 (1990) 301-303.

[21] K. Kneipp, H. Kneipp, I. Itzkan, R.R. Dasari, and M.S. Feld, Ultrasensitive chemical analysis by Raman spectroscopy. Chemical reviews 99 (1999) 2957-2976.

[22] J.W. Chan, D.S. Taylor, T. Zwerdling, S.M. Lane, K. Ihara, and T. Huser, Micro-Raman spectroscopy detects individual neoplastic and normal hematopoietic cells. Biophysical journal 90 (2006) 648-656.

[23] Q. Du, R. Superfine, E. Freysz, and Y. Shen, Vibrational spectroscopy of water at the vapor/water interface. Physical Review Letters 70 (1993) 2313.

[24] J. Dong, J. Malsam, J.C. Bischof, A. Hubel, and A. Aksan, Spatial Distribution of the State of Water in Frozen Mammalian Cells. Biophysical Journal 99 (2010) 2453-2459.

[25] W. Rall, P. Mazur, and J. McGrath, Depression of the ice-nucleation temperature of rapidly cooled mouse embryos by glycerol and dimethyl sulfoxide. Biophysical journal 41 (1983) 1.

[26] P. Mazur, Freezing of living cells: mechanisms and implications. American Journal of Physiology-Cell Physiology 247 (1984) C125-C142.

[27] X. Chen, W. Hua, Z. Huang, and H.C. Allen, Interfacial water structure associated with phospholipid membranes studied by phase-sensitive vibrational sum frequency generation spectroscopy. Journal of the American Chemical Society 132 (2010) 11336-11342.

[28] C. Branca, S. Magazu, G. Maisano, and P. Migliardo, Anomalous cryoprotective effectiveness of trehalose: Raman scattering evidences. The Journal of chemical physics 111 (1999) 281-287.

[29] M.C. Donnamaria, E.I. Howard, and J.R. Grigera, Interaction of water with α, α-trehalose in solution: molecular dynamics simulation approach. Journal of the Chemical Society, Faraday Transactions 90 (1994) 2731-2735.

[30] A. Lerbret, P. Bordat, F. Affouard, M. Descamps, and F. Migliardo, How homogeneous are the trehalose, maltose, and sucrose water solutions? An insight from molecular dynamics simulations. The Journal of Physical Chemistry B 109 (2005) 11046-11057.

[31] J.L. Green, and C.A. Angell, Phase relations and vitrification in saccharide-water solutions and the trehalose anomaly. The Journal of Physical Chemistry 93 (1989) 2880-2882.

[32] S.N. Timasheff, The Control of Protein Stability and Association by Weak Interactions with Water: How Do Solvents Affect These Processes? Annual Review of Biophysics and Biomolecular Structure 22 (1993) 67-97.

[33] T. Uchida, M. Nagayama, and K. Gohara, Trehalose solution viscosity at low temperatures measured by dynamic light scattering method: Trehalose depresses molecular transportation for ice crystal growth. Journal of Crystal Growth 311 (2009) 4747-4752.

[34] M.D. Abràmoff, P.J. Magalhães, and S.J. Ram, Image processing with ImageJ. Biophotonics International 11 (2004) 36-42.

[35] L.J. Belaid, and W. Mourou, Image segmentation: a watershed transformation algorithm. Image Analysis & Stereology 28 (2009) 93-102.

[36] B.T. Storey, E.E. Noiles, and K.A. Thompson, Comparison of glycerol, other polyols, trehalose, and raffinose to provide a defined cryoprotectant medium for mouse sperm cryopreservation. Cryobiology 37 (1998) 46-58.

[37] F. Lang, G.L. Busch, M. Ritter, H. VÖLKL, S. Waldegger, E. Gulbins, and D. HÄUSSINGER, Functional significance of cell volume regulatory mechanisms. Physiological reviews 78 (1998) 247-306.

[38] D. Pegg, The history and principles of cryopreservation, Seminars in reproductive medicine, Copyright© 2002 by Thieme Medical Publishers, Inc., 333 Seventh Avenue, New York, NY 10001, USA. Tel.:+ 1 (212) 584-4662, 2002, pp. 005-014.

[39] W. Rall, Factors affecting the survival of mouse embryos cryopreserved by vitrification. Cryobiology 24 (1987) 387-402.

555 [40] G.M. Fahy, Simplified calculation of cell water content during freezing and thawing in
556 nonideal solutions of cryoprotective agents and its possible application to the study
557 of “solution effects” injury. Cryobiology 18 (1981) 473-482.
558 [41] J.O. Karlsson, E.G. Cravalho, and M. Toner, Intracellular ice formation: causes and
559 consequences. Cryo-Letters 14 (1993) 323-334.
560 [42] A. Fowler, and M. Toner, Cryo-injury and biopreservation. Annals of the new york
561 academy of sciences 1066 (2006) 119-135.
562 [43] M. Schmehl, I. Vazquez, and E. Graham, The effects of nonpenetrating
563 cryoprotectants added to TEST-yolk-glycerol extender on the post-thaw motility of
564 ram spermatozoa. Cryobiology 23 (1986) 512-517.
565 [44] J.L. Hanslick, K. Lau, K.K. Noguchi, J.W. Olney, C.F. Zorumski, S. Mennerick, and
566 N.B. Farber, Dimethyl sulfoxide (DMSO) produces widespread apoptosis in the
567 developing central nervous system. Neurobiology of disease 34 (2009) 1-10.
568 [45] R. Notman, M. Noro, B. O'Malley, and J. Anwar, Molecular basis for dimethylsulfoxide
569 (DMSO) action on lipid membranes. Journal of the American Chemical Society 128
570 (2006) 13982-13983.
571 [46] M.-A. de Ménorval, L.M. Mir, M.L. Fernández, and R. Reigada, Effects of dimethyl
572 sulfoxide in cholesterol-containing lipid membranes: a comparative study of
573 experiments in silico and with cells. PloS one 7 (2012) e41733.
574 [47] G.M. Fahy, T.H. Lilley, H. Linsdell, M.S.J. Douglas, and H.T. Meryman,
575 Cryoprotectant toxicity and cryoprotectant toxicity reduction: in search of molecular
576 mechanisms. Cryobiology 27 (1990) 247-268.

[48] S.K. Singh, P. Kolhe, A.P. Mehta, S.C. Chico, A.L. Lary, and M. Huang, Frozen state storage instability of a monoclonal antibody: Aggregation as a consequence of trehalose crystallization and protein unfolding. Pharmaceutical research 28 (2011) 873-885.

[49] Y. Momose, R. Matsumoto, A. Maruyama, and M. Yamaoka, Comparative analysis of transcriptional responses to the cryoprotectants, dimethyl sulfoxide and trehalose, which confer tolerance to freeze–thaw stress in Saccharomyces cerevisiae. Cryobiology 60 (2010) 245-261.

[50] J.P.R. Motta, F.H. Paraguassú-Braga, L.F. Bouzas, and L.C. Porto, Evaluation of intracellular and extracellular trehalose as a cryoprotectant of stem cells obtained from umbilical cord blood. Cryobiology 68 (2014) 343-348.

[51] L.M. Crowe, D.S. Reid, and J.H. Crowe, Is trehalose special for preserving dry biomaterials? Biophysical journal 71 (1996) 2087.

[52] E. Katenz, F.W.R. Vondran, R. Schwartlander, G. Pless, X. Gong, X. Cheng, P. Neuhaus, and I.M. Sauer, Cryopreservation of primary human hepatocytes: the benefit of trehalose as an additional cryoprotective agent. Liver transplantation 13 (2007) 38-45.

[53] G.M. Beattie, J.H. Crowe, A.D. Lopez, V. Cirulli, C. Ricordi, and A. Hayek, Trehalose: a cryoprotectant that enhances recovery and preserves function of human pancreatic islets after long-term storage. Diabetes 46 (1997) 519-523.

[54] J.H. Crowe, J.S. Clegg, and L.M. Crowe, Anhydrobiosis: the water replacement hypothesis, The Properties of Water in Foods ISOPOW 6, Springer, 1998, pp. 440-455.

[55] C. Erkut, S. Penkov, K. Fahmy, and T.V. Kurzchalia, How worms survive desiccation: Trehalose pro water, Worm, Taylor & Francis, 2012, pp. 61-65.

[56] K. Muldrew, and L.E. McGann, The osmotic rupture hypothesis of intracellular freezing injury. Biophysical Journal 66 (1994) 532.

[57] J. Huebinger, H.-M. Han, O. Hofnagel, I.R. Vetter, P.I. Bastiaens, and M. Grabenbauer, Direct Measurement of Water States in Cryopreserved Cells Reveals Tolerance toward Ice Crystallization. Biophysical journal 110 (2016) 840-849.

[58] K. Brockbank, F. Lightfoot, Y.C. Song, and M. Taylor, Interstitial ice formation in cryopreserved homografts: a possible cause of tissue deterioration and calcification in vivo. The Journal of heart valve disease 9 (2000) 200-206.

[59] B. Minceva-Sukarova, W. Sherman, and G. Wilkinson, The Raman spectra of ice (Ih, II, III, V, VI and IX) as functions of pressure and temperature. Journal of Physics C: Solid State Physics 17 (1984) 5833.

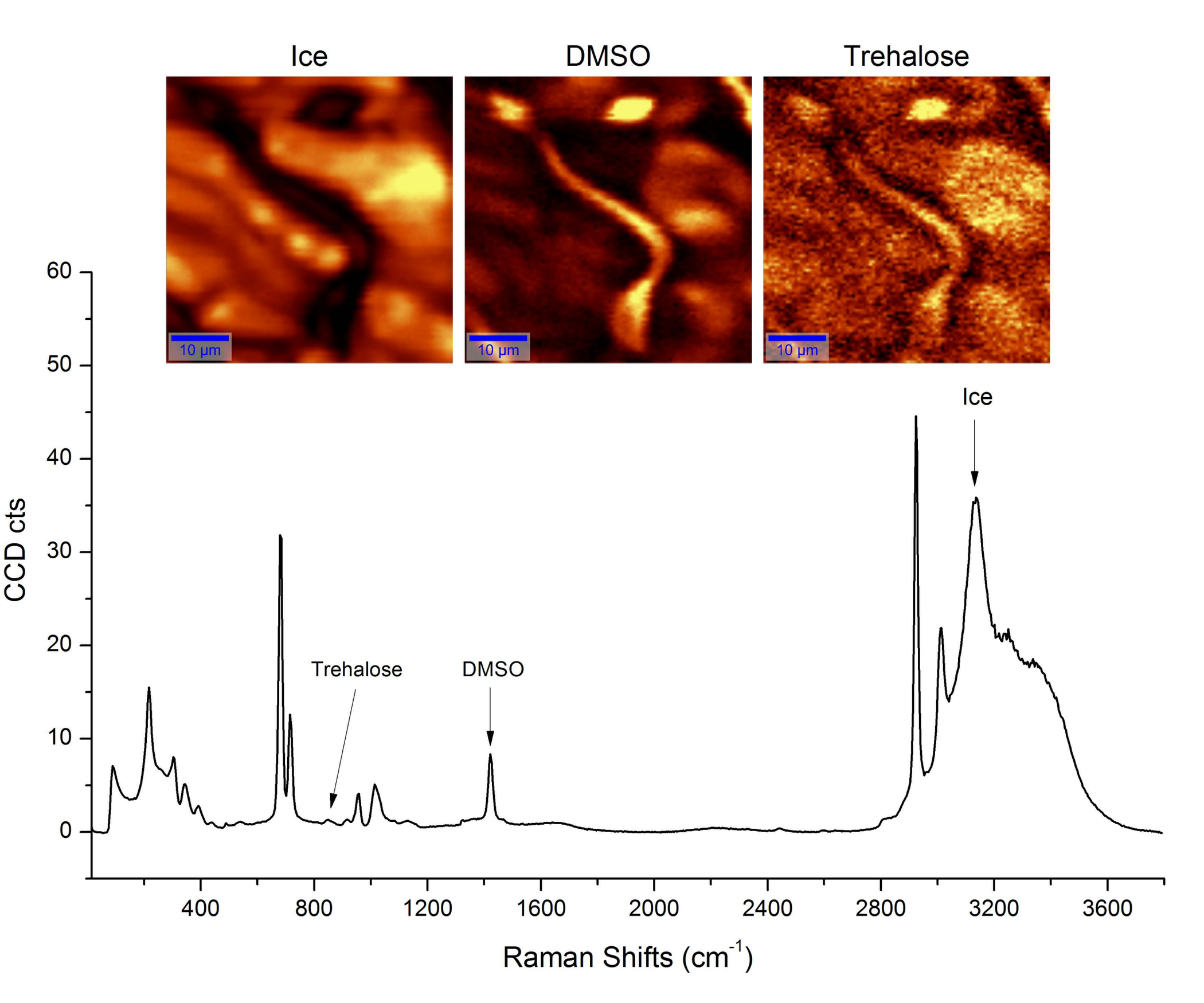
Ice
DMSO
Trehalose
10 µm
10 µm
10 µm
Ice
Trehalose
DMSO
CCD cts
0
10
20
30
40
50
60
400
800
1200
1600
2000
2400
2800
3200
3600
Raman Shifts (cm-1)

10% DMSO +
300mM Trehalose

10% DMSO +
100mM Trehalose

10% DMSO

-40°C

-80°C

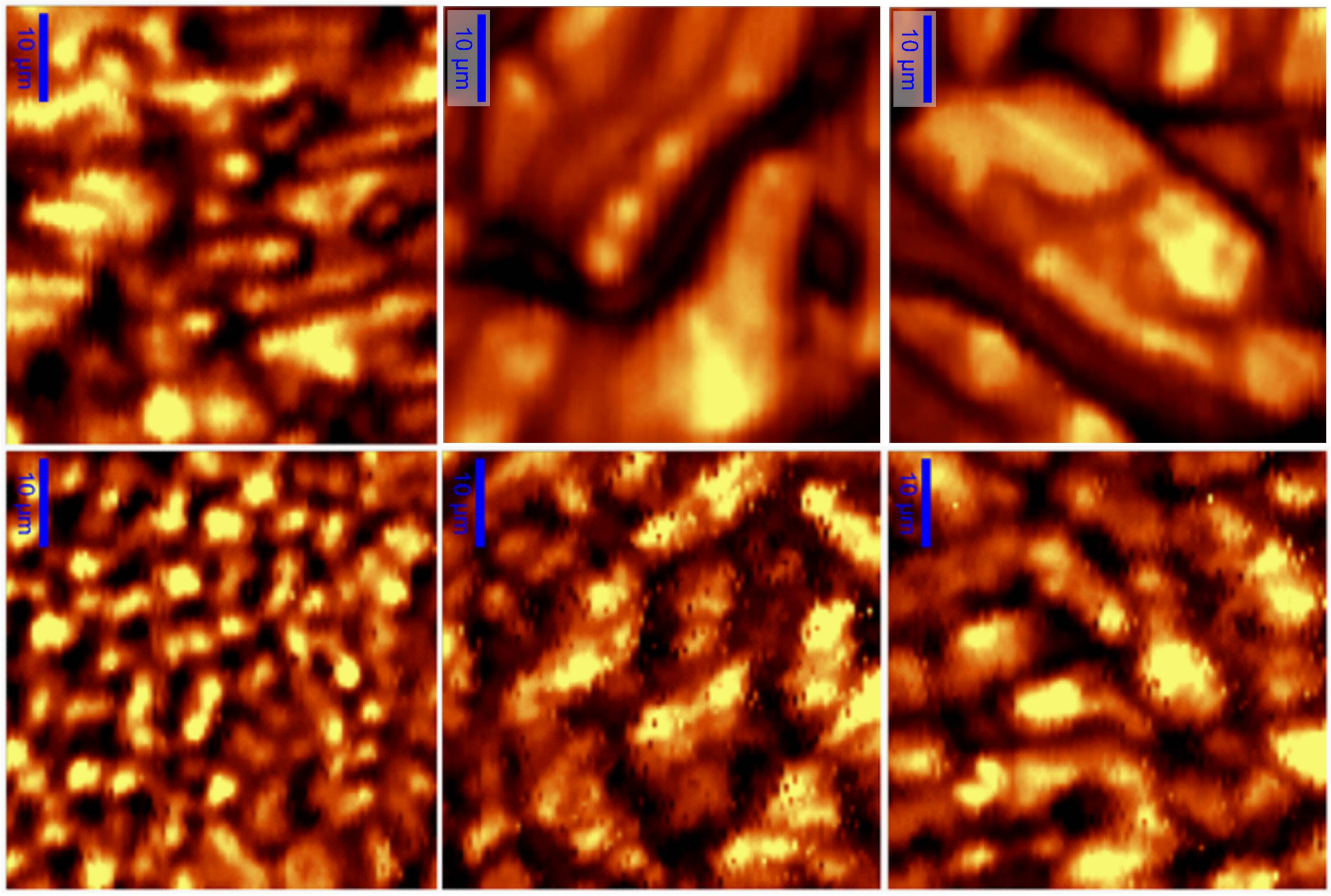

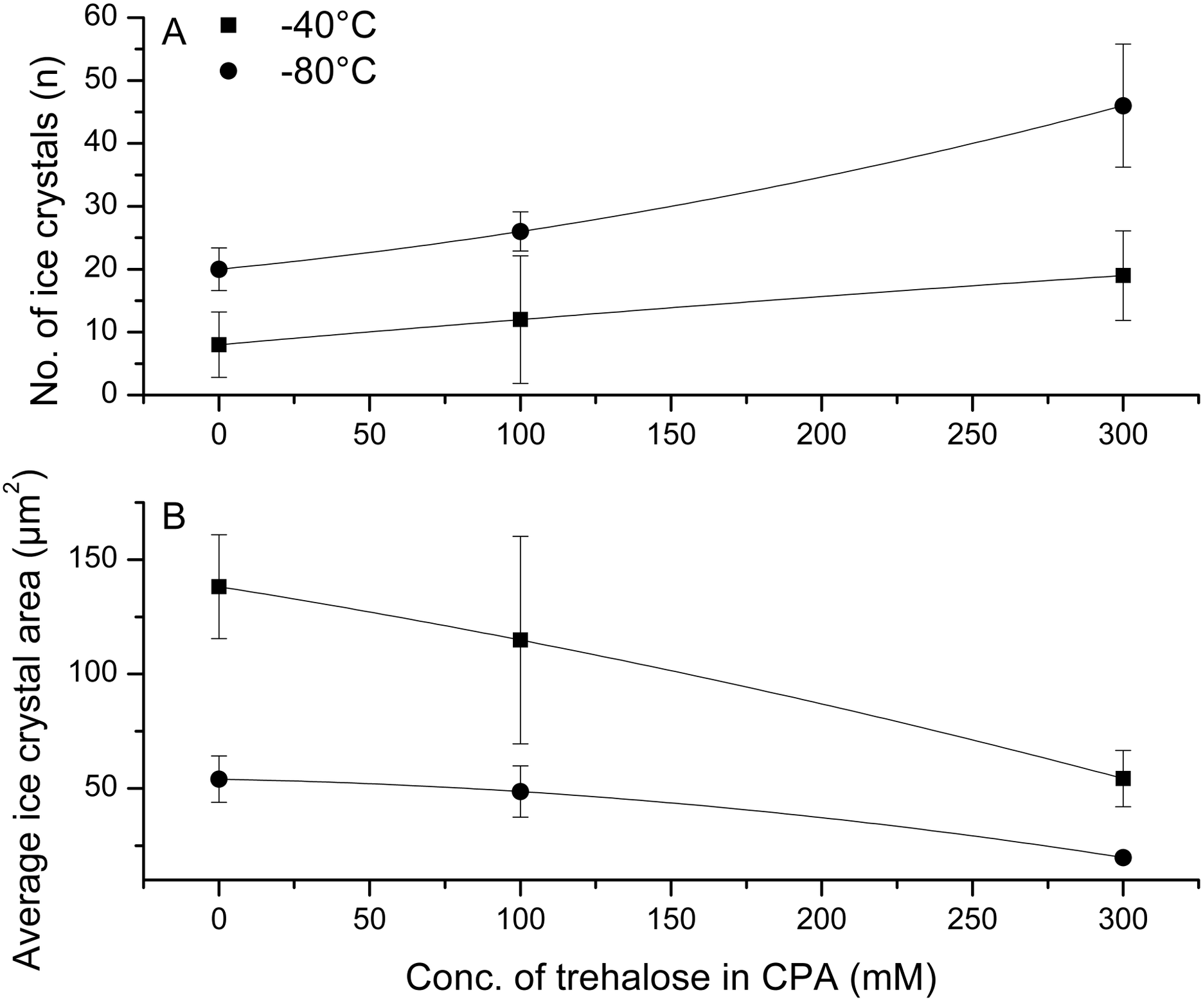
A
-40°C
-80°C
No. of ice crystals (n)
0
10
20
30
40
50
60
0
50
100
150
200
250
300
B
Average ice crystal area (μm²)
50
100
150
0
50
100
150
200
250
300
Conc. of trehalose in CPA (mM)

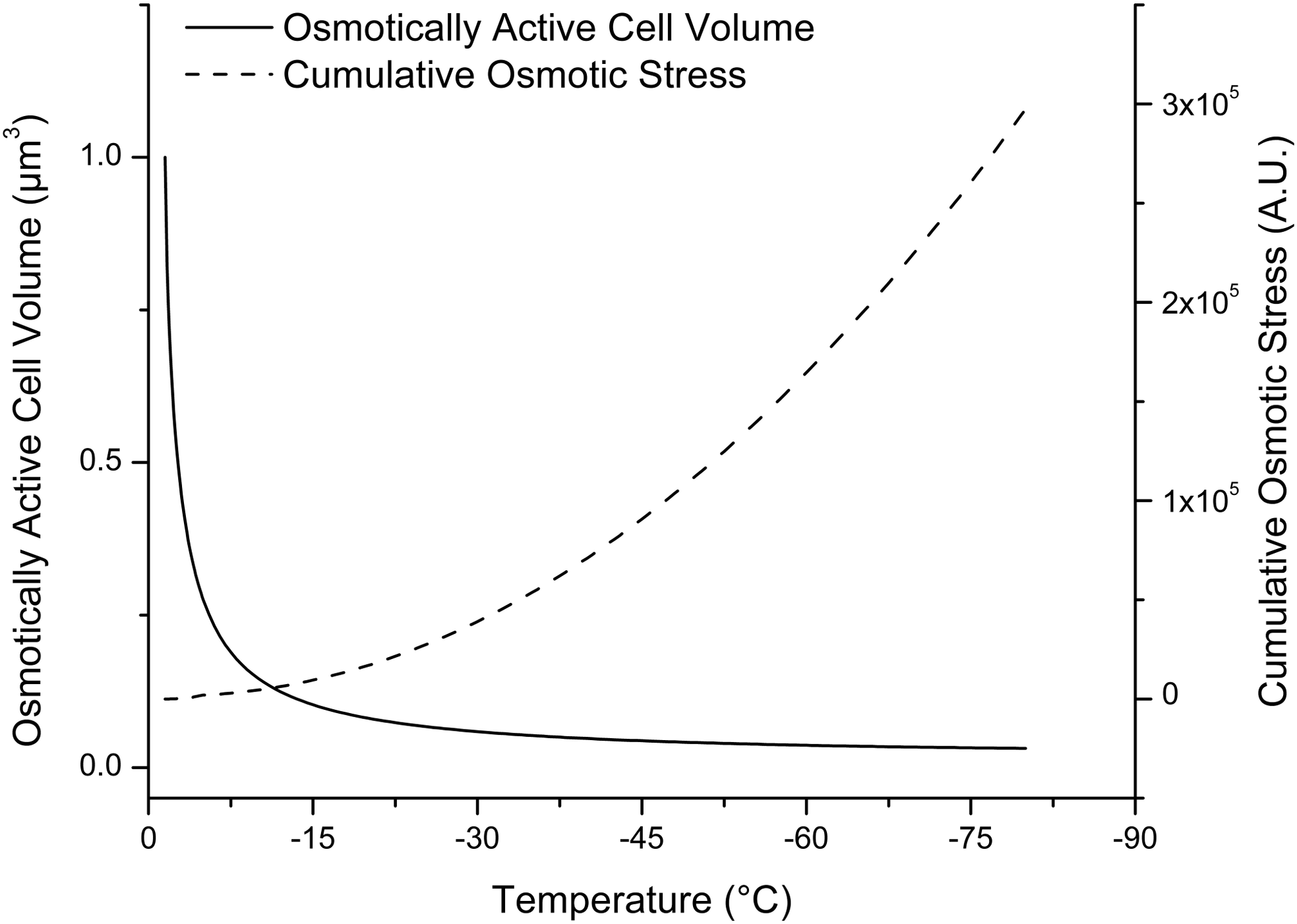
Osmotically Active Cell Volume
Cumulative Osmotic Stress
Osmotically Active Cell Volume (μm3)
1.0
0.5
0.0
3x10^5
2x10^5
1x10^5
0
Cumulative Osmotic Stress (A.U.)
0
-15
-30
-45
-60
-75
-90
Temperature (°C)

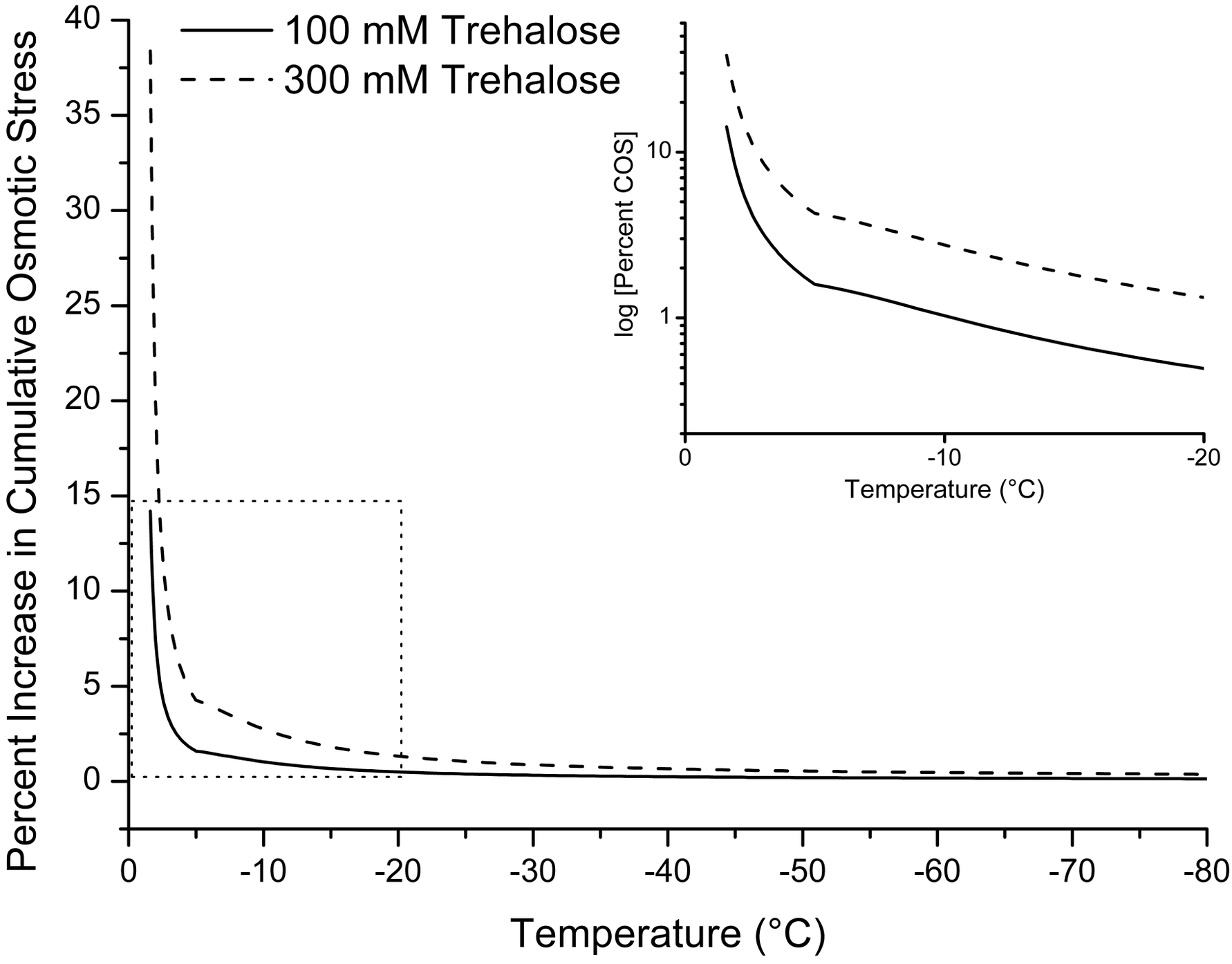
100 mM Trehalose
300 mM Trehalose
Percent Increase in Cumulative Osmotic Stress
40
35
30
25
20
15
10
5
0
0
-10
-20
-30
-40
-50
-60
-70
-80
Temperature (°C)
log [Percent COS]
10
1
0
-10
-20
Temperature (°C)

A

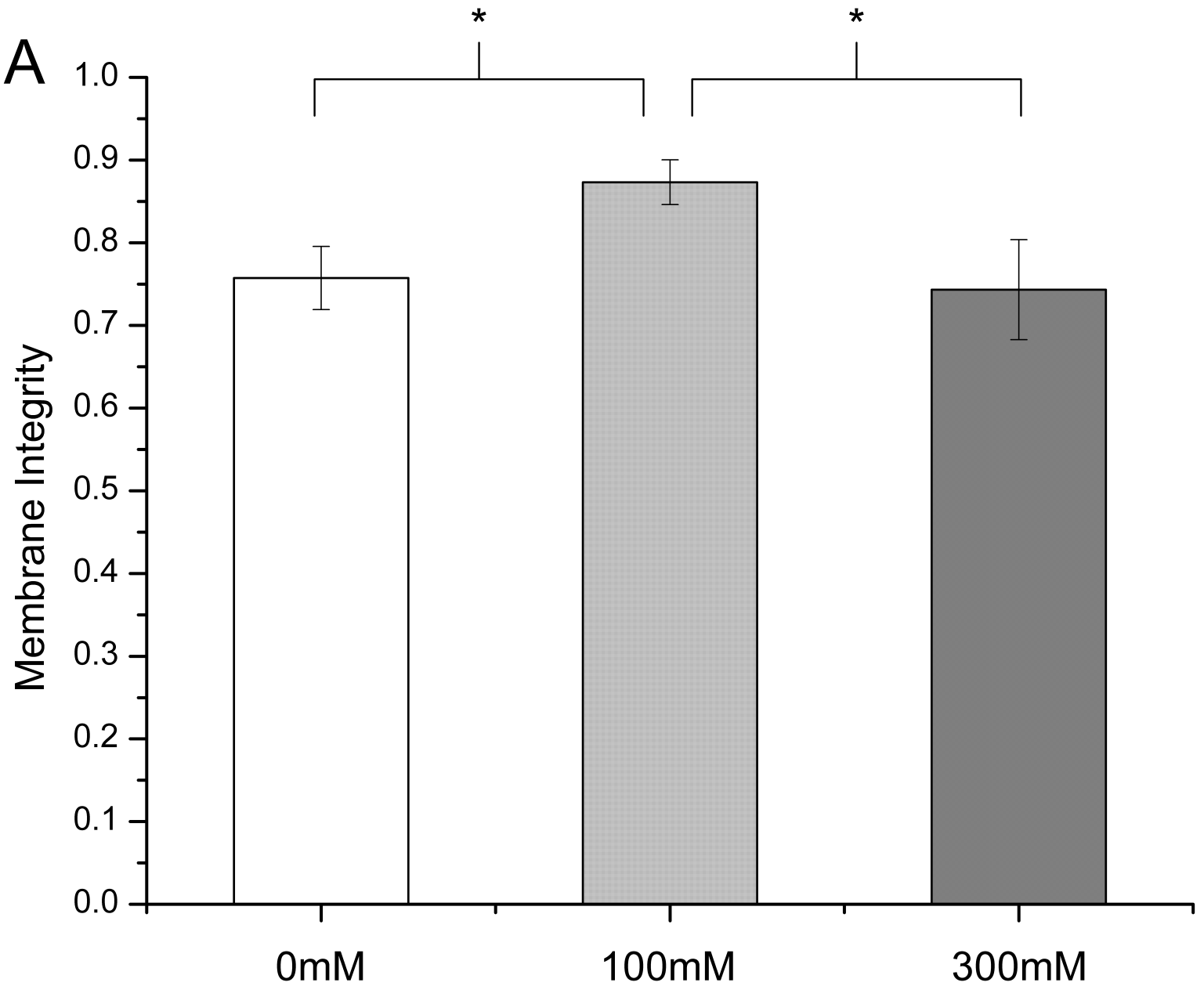
*
*
1.0
0.9
0.8
0.7
0.6
0.5
0.4
0.3
0.2
0.1
0.0
Membrane Integrity
0mM
100mM
300mM

B

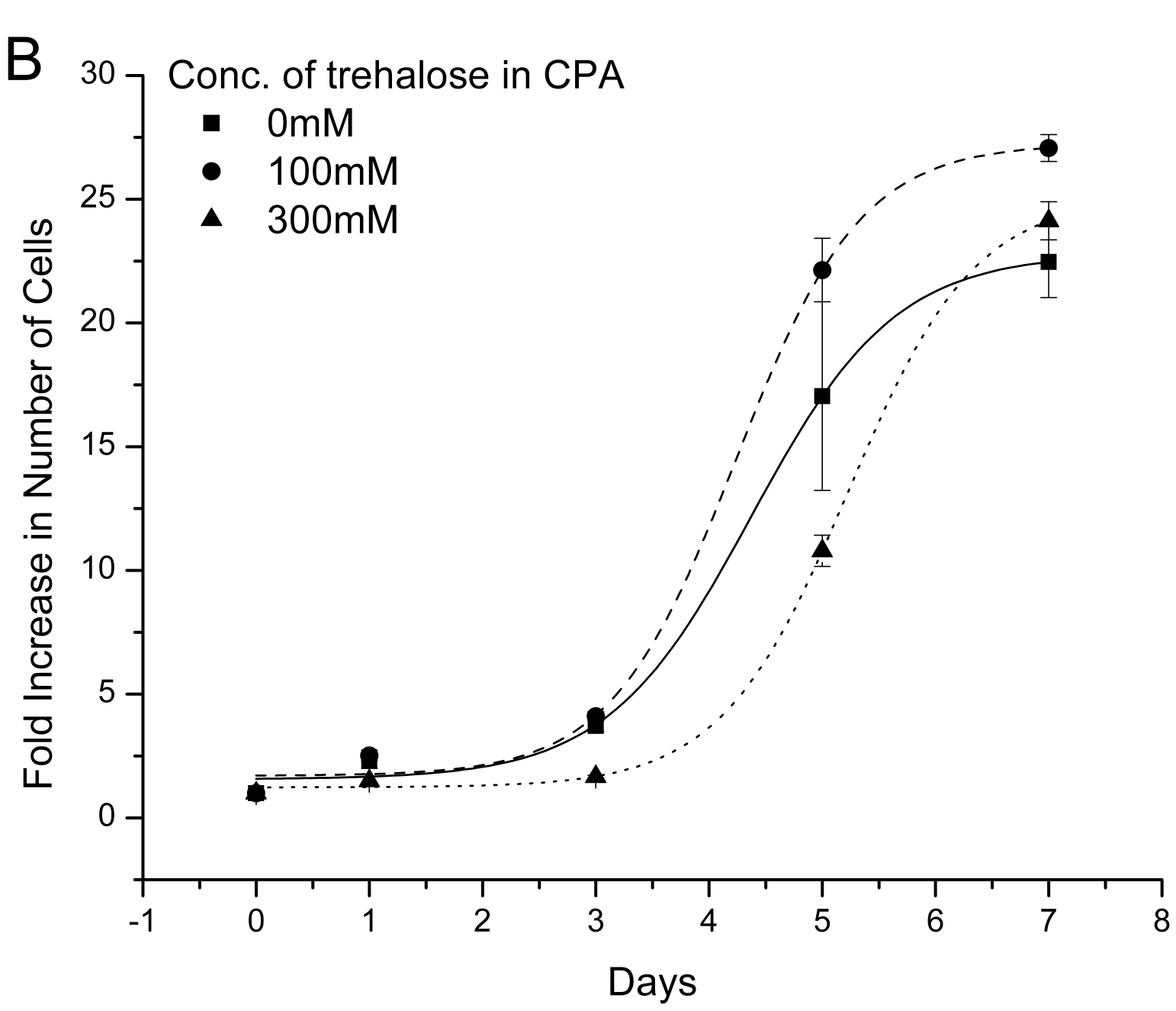
Conc. of trehalose in CPA
0mM
100mM
300mM
30
25
20
15
10
5
0
Fold Increase in Number of Cells
-1
0
1
2
3
4
5
6
7
8
Days

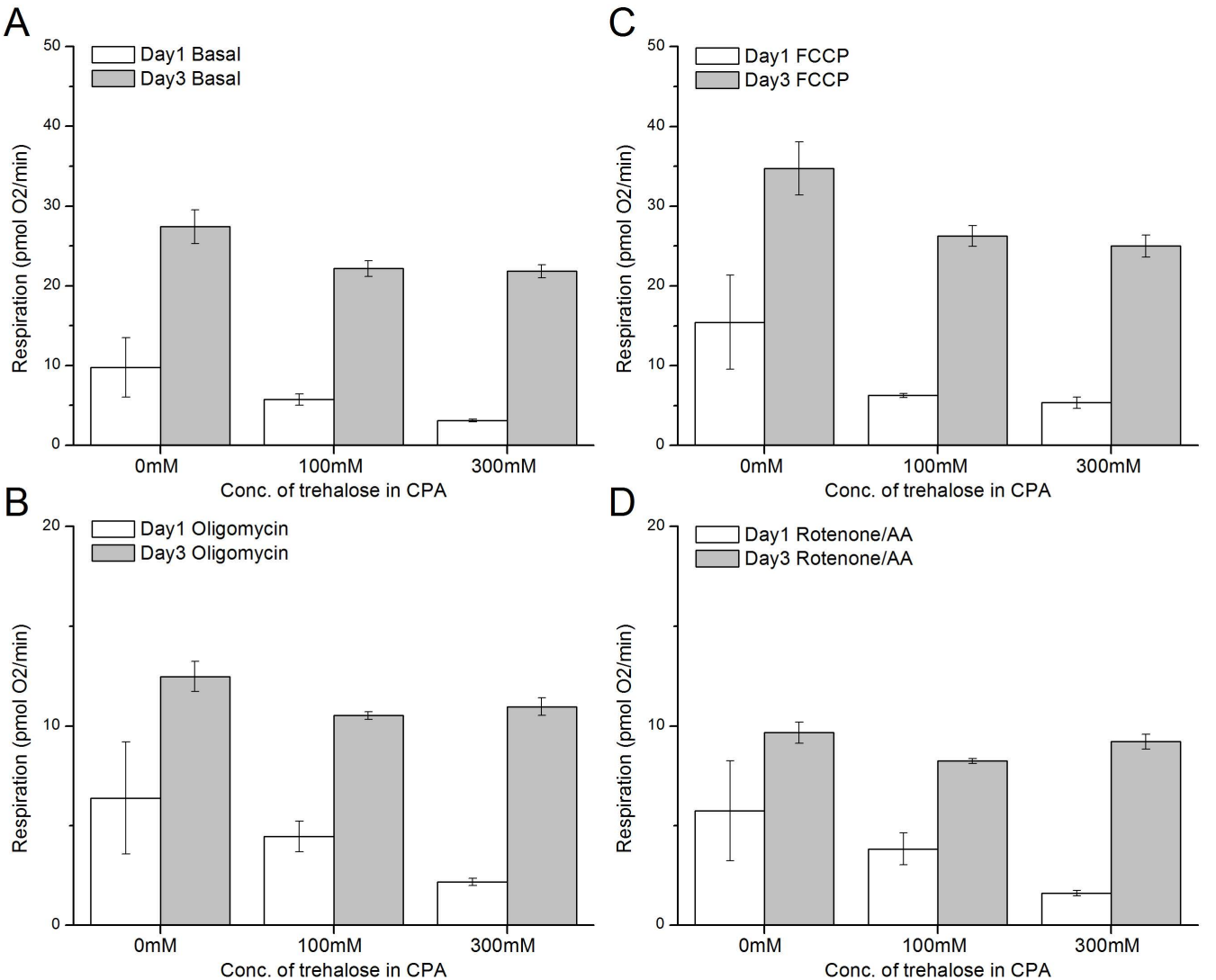
A
Day1 Basal
Day3 Basal
Respiration (pmol O2/min)
0
10
20
30
40
50
0mM
100mM
300mM
Conc. of trehalose in CPA
B
Day1 Oligomycin
Day3 Oligomycin
Respiration (pmol O2/min)
0
10
20
0mM
100mM
300mM
Conc. of trehalose in CPA
C
Day1 FCCP
Day3 FCCP
Respiration (pmol O2/min)
0
10
20
30
40
50
0mM
100mM
300mM
Conc. of trehalose in CPA
D
Day1 Rotenone/AA
Day3 Rotenone/AA
Respiration (pmol O2/min)
0
10
20
0mM
100mM
300mM
Conc. of trehalose in CPA